9. I. A. Adzhubei *et al.*, *Nat. Methods* **7**, 248–249 (2010).
10. P. C. Ng, S. Henikoff, *Nucleic Acids Res.* **31**, 3812–3814 (2003).
11. D. Welter *et al.*, *Nucleic Acids Res.* **42**, D1001–D1006 (2014).
12. D. M. Ibrahim *et al.*, *Genome Res.* **23**, 2091–2102 (2013).
13. M. F. Berger *et al.*, *Nat. Biotechnol.* **24**, 1429–1435 (2006).
14. B. Jiang, J. S. Liu, M. L. Bulyk, *Bioinformatics* **29**, 1390–1398 (2013).
15. J. I. Fuxman Bass *et al.*, *Cell* **161**, 661–673 (2015).
16. C. L. Freund *et al.*, *Cell* **91**, 543–553 (1997).
17. A. Swaroop *et al.*, *Hum. Mol. Genet.* **8**, 299–305 (1999).
18. P. K. Swain *et al.*, *Neuron* **19**, 1329–1336 (1997).
19. N. Brison, P. Debeer, P. Tylzanowski, *Dev. Dyn.* **243**, 37–48 (2014).
20. V. Salsi, M. A. Vigano, F. Cocchiarella, R. Mantovani, V. Zappavigna, *Dev. Biol.* **317**, 497–507 (2008).
21. P. Sulem *et al.*, *Nat. Genet.* **47**, 448–452 (2015).
22. M. Ouedraogo *et al.*, *PLOS ONE* **7**, e50653 (2012).
23. T. Lappalainen, S. B. Montgomery, A. C. Nica, E. T. Dermitzakis, *Am. J. Hum. Genet.* **89**, 459–463 (2011).

ACKNOWLEDGMENTS

We thank M. Hume, Y.-H. Hsu, Y. Shen, and D. Balcha for technical assistance and A. Gimelbrant for helpful discussions. We are grateful to the Exome Aggregation Consortium for making its data publicly available prior to publication. This work was supported by the National Institutes of Health (grants NHGRI R01 HG003985 to M.L.B. and T.H. and P50 HG004233 to M.V. and D.E.H.), an A*STAR National Science Scholarship to K.H.K., and National Science Foundation Graduate Research Fellowships to L.A.B. and J.M.R. TF PBM data have been deposited into UniPROBE (publication data set accession BAR15A). GST negative control PBM 8-mer data are provided in table S7. M.L.B. is a coinventor on U.S. patents no. 6,548,021 and no. 8,530,638 on PBM technology and corresponding universal sequence designs, respectively. Universal PBM array designs used in this study are available via a materials transfer agreement with The Brigham and Women's Hospital. A.V., J.V.K., J.M.R., N.S., T.H., and S.Y. performed experiments; L.A.B., J.V.K., J.M.R., S.S.G., E.J.R., J.W., L.M., K.H.K., S.I., T.S., L.S., R.G., and C.C. performed data analysis; M.K., M.J.D., M.V., D.E.H., and M.L.B. supervised research; L.A.B., L.M., K.H.K., D.E.H., and M.L.B. designed the study and wrote the manuscript; and L.A.B., J.V.K., J.M.R., S.S.G., L.M., K.H.K., S.I., and M.L.B. prepared figures and tables.

SUPPLEMENTARY MATERIALS

www.sciencemag.org/content/351/6280/1450/suppl/DC1
Materials and Methods
Figs. S1 to S12
Tables S1 to S7
References (*24*–*55*)

21 September 2015; accepted 18 February 2016
10.1126/science.aad2257

CANCER

Activation of proto-oncogenes by disruption of chromosome neighborhoods

Denes Hnisz,[1]* Abraham S. Weintraub,[1,2]* Daniel S. Day,[1] Anne-Laure Valton,[3] Rasmus O. Bak,[4] Charles H. Li,[1,2] Johanna Goldmann,[1] Bryan R. Lajoie,[3] Zi Peng Fan,[1,5] Alla A. Sigova,[1] Jessica Reddy,[1,2] Diego Borges-Rivera,[1,2] Tong Ihn Lee,[1] Rudolf Jaenisch,[1,2] Matthew H. Porteus,[4] Job Dekker,[3,6] Richard A. Young[1,2]†

Oncogenes are activated through well-known chromosomal alterations such as gene fusion, translocation, and focal amplification. In light of recent evidence that the control of key genes depends on chromosome structures called insulated neighborhoods, we investigated whether proto-oncogenes occur within these structures and whether oncogene activation can occur via disruption of insulated neighborhood boundaries in cancer cells. We mapped insulated neighborhoods in T cell acute lymphoblastic leukemia (T-ALL) and found that tumor cell genomes contain recurrent microdeletions that eliminate the boundary sites of insulated neighborhoods containing prominent T-ALL proto-oncogenes. Perturbation of such boundaries in nonmalignant cells was sufficient to activate proto-oncogenes. Mutations affecting chromosome neighborhood boundaries were found in many types of cancer. Thus, oncogene activation can occur via genetic alterations that disrupt insulated neighborhoods in malignant cells.

Tumor cell gene expression programs are typically driven by somatic mutations that alter the coding sequence or expression of proto-oncogenes (*1*) (Fig. 1A), and identifying such mutations in patient genomes is a major goal of cancer genomics (*2*, *3*). Dysregulation of proto-oncogenes frequently involves mutations that bring transcriptional enhancers into proximity of these genes (*4*). Transcriptional enhancers normally interact with their target genes through the formation of DNA loops (*5*–*7*), which typically are constrained within larger CCCTC-binding factor (CTCF) cohesin–mediated loops called insulated neighborhoods (*8*–*10*), which in turn can form clusters that contribute to topologically associating domains (TADs) (*11*, *12*) (fig. S1A). This recent understanding of chromosome structure led us to hypothesize that silent proto-oncogenes located within insulated neighborhoods might be activated in cancer cells via loss of an insulated neighborhood boundary, with consequent aberrant activation by enhancers that are normally located outside the neighborhood (Fig. 1A, lowest panel).

To test this hypothesis, we used chromatin interaction analysis by paired-end tag sequencing (ChIA-PET) to map neighborhoods and other cis-regulatory interactions in a cancer cell genome (Fig. 1B and table S1). A T cell acute lymphoblastic leukemia (T-ALL) Jurkat cell line was selected for these studies because key T-ALL oncogenes and genetic alterations are well known (*13*, *14*). The ChIA-PET technique generates a high-resolution (~5 kb) chromatin interaction map of sites in the genome bound by a specific protein factor (*8*, *15*, *16*). Cohesin was selected as the target protein because it is involved in both CTCF-CTCF interactions and enhancer-promoter interactions (*5*–*7*) and has proven useful for identifying insulated neighborhoods (*8*, *10*) (fig. S1, A and B). The cohesin ChIA-PET data were processed using multiple analytical approaches (figs. S1 to S4 and table S2), and their analysis identified 9757 high-confidence interactions, including 9038 CTCF-CTCF interactions and 379 enhancer-promoter interactions (fig. S4C). The CTCF-CTCF loops had a median length of 270 kb, contained on average two or three genes, and covered ~52% of the genome (table S2). Such CTCF-CTCF loops have been called insulated neighborhoods because disruption of either CTCF boundary causes dysregulation of local genes due to inappropriate enhancer-promoter interactions (*8*, *10*). Consistent with this, the Jurkat chromosome structure data showed that the majority of cohesin-associated enhancer-promoter interactions had end points that occurred within the CTCF-CTCF loops (Fig. 1C and fig. S2H). These results provide an initial map of the three-dimensional (3D) regulatory landscape of a tumor cell genome.

We next investigated the relationship between genes that have been implicated in T-ALL pathogenesis and the insulated neighborhoods. The majority of genes (40 of 55) implicated in T-ALL pathogenesis, as curated from the Cancer Gene Census and individual studies (table S3), were located within the insulated neighborhoods identified in Jurkat cells (Fig. 2A and fig. S5); 27 of these genes were transcriptionally active and 13 were silent, as determined by RNA sequencing (RNA-seq) (Fig. 2A and table S4). Active oncogenes are often associated with super-enhancers (*17*, *18*), and we found that 13 of the 27 active T-ALL pathogenesis genes were associated with superenhancers (Fig. 2, A and B, and fig. S5A). Silent genes have also been shown to be protected by insulated neighborhoods from active enhancers located outside the neighborhood, and we found multiple instances of silent proto-oncogenes located within CTCF-CTCF loop structures in the Jurkat genome (Fig. 2, A and C, and fig. S5B). Thus, both active oncogenes and

[1]Whitehead Institute for Biomedical Research, Cambridge, MA 02142, USA. [2]Department of Biology, Massachusetts Institute of Technology, Cambridge, MA 02139, USA. [3]Program in Systems Biology, Department of Biochemistry and Molecular Pharmacology, University of Massachusetts Medical School, Worcester, MA 01605, USA. [4]Department of Pediatrics, Stanford University, Stanford, CA, USA. [5]Computational and Systems Biology Program, Massachusetts Institute of Technology, Cambridge, MA 02139, USA. [6]Howard Hughes Medical Institute.
*These authors contributed equally to this work. †Corresponding author. E-mail: young@wi.mit.edu

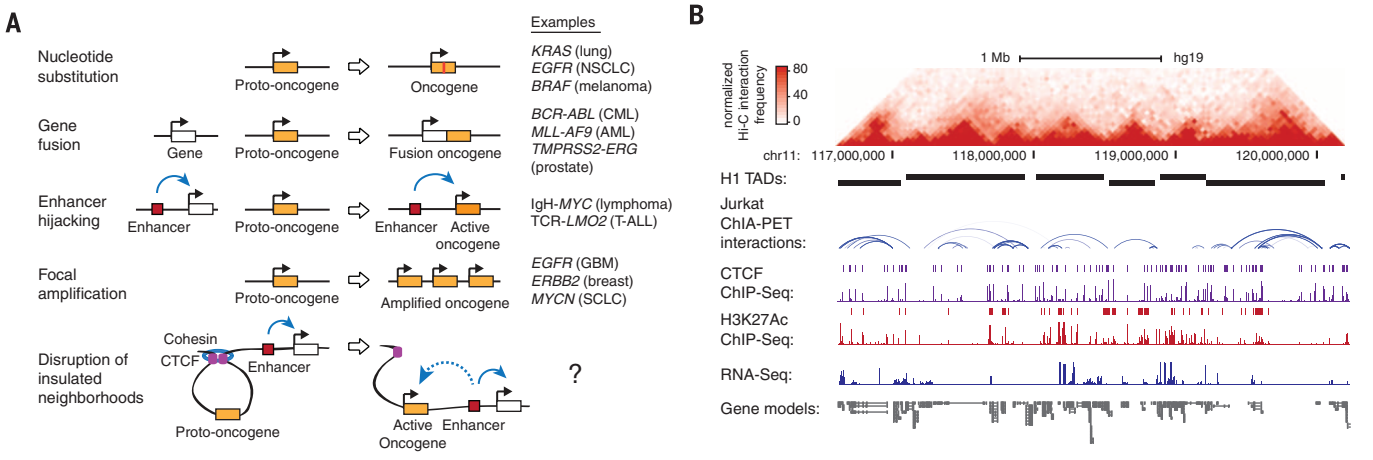

Fig. 1. 3D regulatory landscape of the T-ALL genome. (**A**) Mechanisms activating proto-oncogenes. (**B**) Hi-C interaction map, TADs defined in human embryonic stem cells (H1), cohesin ChIA-PET interactions (intensity of blue arc represents interaction significance), CTCF and H3K27Ac chromatin immunoprecipitation sequencing (ChIP-seq) profiles and peaks, and RNA-seq in Jurkat cells at the *CD3D* locus. ChIP-seq peaks are denoted as bars above ChIP-seq profiles. (**C**) ChIA-PET interactions at the *RUNX1* locus displayed above the ChIP-seq profiles of CTCF, cohesin (SMC1), and H3K27Ac. FDR, false discovery rate.

silent proto-oncogenes are located within insulated neighborhoods in these T-ALL cells.

If some insulated neighborhoods function to prevent proto-oncogene activation, some T-ALL tumor cells may have genetic alterations that perturb the CTCF boundaries of neighborhoods containing T-ALL oncogenes. To investigate this possibility, we identified recurrent deletions in T-ALL genomes that span insulated neighborhood boundaries, using data from multiple studies (table S5A) and filtered for relatively short deletions (<500 kb) so as to minimize collection of deletions that affect multiple genes (fig. S6A). Among the 438 recurrent deletions identified with this approach, 113 overlapped at least one boundary of insulated neighborhoods identified in T-ALL, and 6 of these affected neighborhoods containing T-ALL pathogenesis genes (fig. S6B and table S5B). Examples of two such genes, *TAL1* and *LMO2*, are shown in Fig. 3, A and G.

If deletions overlapping neighborhood boundaries can cause activation of proto-oncogenes within the loops, then site-specific deletion of a loop boundary CTCF site at the *TAL1* locus should be sufficient to activate these proto-oncogenes in nonmalignant cells. *TAL1* encodes a transcription factor that is overexpressed in ~50% of T-ALL cases and is a key oncogenic driver of this cancer (*19*, *20*). *TAL1* can be activated by deletions that fuse a promoterless *TAL1* gene to the promoter of *STIL* (*19*), and this was observed in many patient deletions (Fig. 3A). Several patient deletions, however, retained the *TAL1* promoter

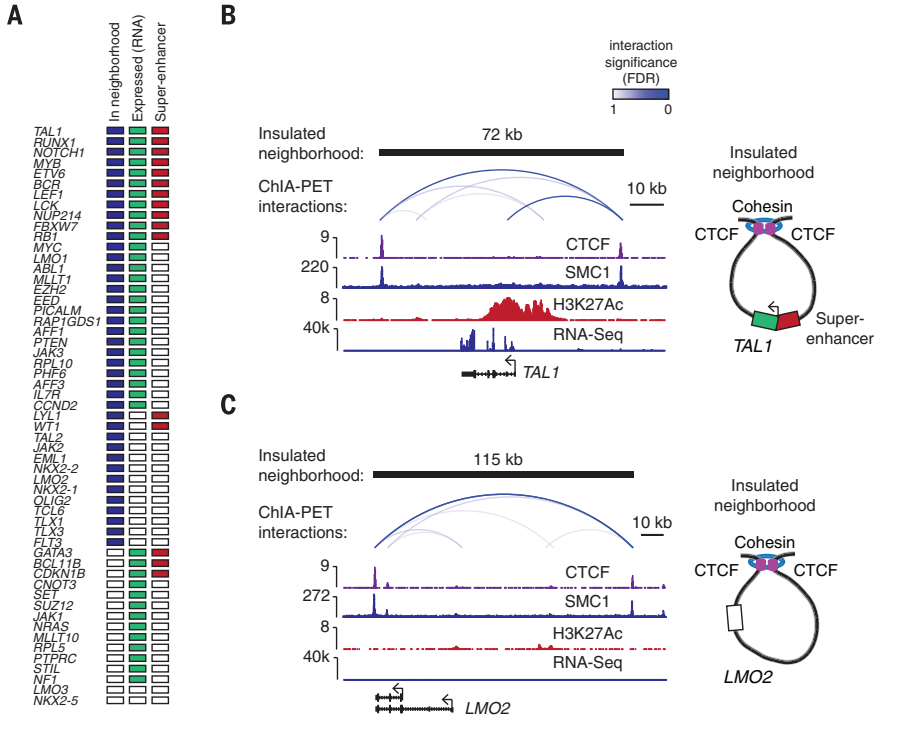

Fig. 2. Active oncogenes and silent proto-oncogenes occur in insulated neighborhoods. (**A**) T-ALL pathogenesis genes. Colored boxes indicate whether a gene is located within a neighborhood, expressed, and associated with a superenhancer. (**B**) Insulated neighborhood at the active *TAL1* locus. The cohesin ChIA-PET interactions are displayed above the ChIP-seq profiles of CTCF, cohesin (SMC1) H3K27Ac, and RNA-seq profile. A model of the insulated neighborhood is shown on the right. (**C**) Insulated neighborhood at the silent *LMO2* locus.

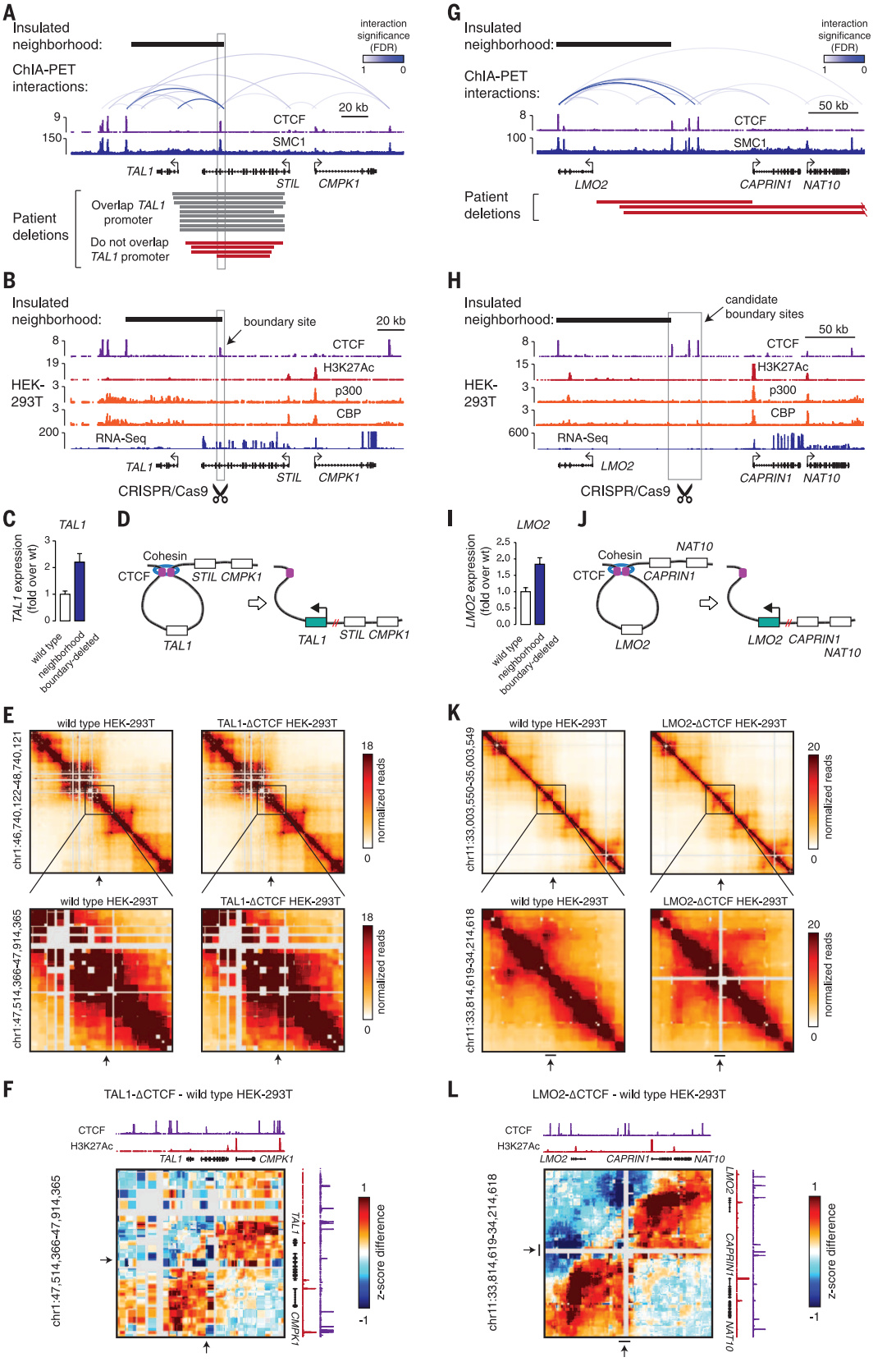

Fig. 3. Disruption of insulated neighborhood boundaries is linked to proto-oncogene activation. (**A**) Cohesin ChIA-PET interactions and CTCF and cohesin (SMC1) binding profiles at the *TAL1* locus in Jurkat cells. Patient deletions described in (*22*) are shown as bars below the gene models. The deletion on the bottom indicates the minimally deleted region identified in (*26*). (**B**) ChIP-seq profiles of CTCF, H3K27Ac, p300, CBP, and RNA-seq at the *TAL1* locus in HEK-293T cells. The region deleted using a CRISPR/Cas9-based approach is highlighted in a gray box. (**C**) Quantitative reverse transcription polymerase chain reaction (qRT-PCR) analysis of *TAL1* expression in wild-type HEK-293T cells (wt) and in cells where the neighborhood boundary highlighted in (B) was deleted. (**D**) Model of the neighborhood and perturbation at the *TAL1* locus. (**E**) 5C contact matrices in wild-type HEK-293T cells and TAL1 neighborhood boundary–deleted cells. An arrow indicates the position of the region removed in the mutant cells. (**F**) Distance-adjusted z-score difference (5C) maps at the *TAL1* locus (ΔCTCF – wild-type HEK-293T). Note the increase in the 5C signal adjacent to the deleted region. CTCF and H3K27Ac binding profiles in wild-type cells are displayed for orientation. (**G**) Cohesin ChIA-PET interactions and CTCF and cohesin (SMC1) binding profiles at the *LMO2* locus. Patient deletions described in (*22*) are shown as bars below the gene models. (**H**) ChIP-Seq binding profile of CTCF, H3K27Ac, p300, CBP, and RNA-seq at the *LMO2* locus in HEK-293T cells. The region deleted by a CRISPR/Cas9-based approach is highlighted in a gray box. (**I**) qRT-PCR analysis of *LMO2* expression in wild-type HEK-293T cells and in cells where the neighborhood boundary highlighted in (H) was deleted. (**J**) Model of the neighborhood and perturbation at the *LMO2* locus. (**K**) 5C contact matrices in wild-type HEK-293T cells and LMO2 neighborhood boundary–deleted cells. An arrow indicates the position of the region removed in the mutant cells. (**L**) Distance-adjusted z-score difference (5C) maps at the *LMO2* locus (ΔCTCF – wild-type HEK-293T). Note the increase in the 5C signal adjacent to the deleted region. CTCF and H3K27Ac binding profiles in wild-type cells are displayed for orientation. In (C) and (I), data from $n = 3$ independent biological replicates are displayed as means ± SD; $P < 0.01$ between wild-type and boundary-deleted cells (two-tailed t test).

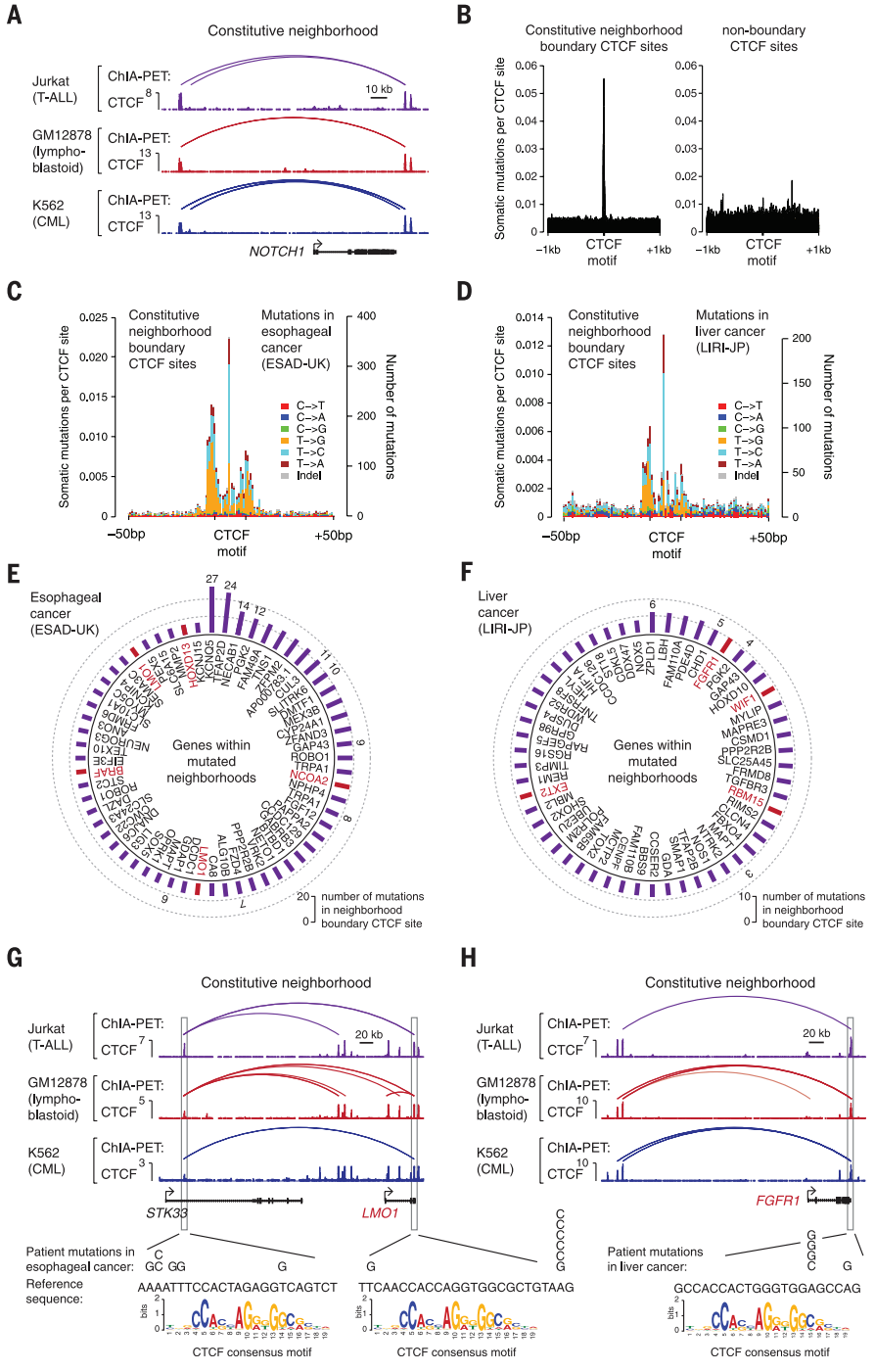

Fig. 4. Somatic mutations of neighborhood boundaries occur in many cancers. (**A**) "Constitutive neighborhood" at the *NOTCH1* locus. CTCF ChIP-seq and cohesin ChIA-PET interactions in Jurkat (T-ALL), GM12878 (lymphoblastoid), and K562 (CML) cells are displayed. (**B**) Frequency of somatic mutations in the ICGC database at CTCF sites that form constitutive neighborhood boundaries (left) and CTCF sites that do not form neighborhood boundaries (right). (**C**) Somatic mutations in esophageal adenocarcinoma (ESAD-UK) at constitutive neighborhood boundary CTCF sites. (**D**) Somatic mutations in hepatocellular carcinoma (LIRI-JP) at constitutive neighborhood boundary CTCF sites. (**E** and **F**) Genes in constitutive neighborhoods whose boundary is recurrently mutated in esophageal adenocarcinoma (E) and in hepatocellular carcinoma (F). The bars depict the number of mutations in the neighborhood boundary site. Proto-oncogenes annotated in the Cancer Gene Census are highlighted in red. (**G** and **H**) Mutations in the boundary sites of the neighborhood containing the *LMO1* proto-oncogene in esophageal adenocarcinoma (G) and the *FGFR1* proto-oncogene in hepatocellular carcinoma (H). The enrichment of mutations at the constitutive neighborhood boundary sites (±5 bp of the motif) shown in (B) to (D) relative to regions flanking the binding sites has a *P* value of $<10^{-4}$ (permutation test).

(end point >5 kb from promoter) but overlapped the CTCF boundary site of the *TAL1* neighborhood (Fig. 3A), and *TAL1* was active in the samples harboring these deletions (fig. S7, A and B). This suggests disruption of the insulated neighborhood, allowing activation of *TAL1* by regulatory elements outside of the loop.

We tested this idea by CRISPR/Cas9-mediated deletion of the *TAL1* neighborhood boundary in human embryonic kidney (HEK-293T) cells (Fig. 3B). In these cells the *TAL1* proto-oncogene is silent, as evidenced by low H3K27Ac (histone H3 acetylated Lys^{27}) occupancy and RNA-seq (Fig. 3B). However, at least one active regulatory element occurs ~60 kb upstream of *TAL1,* adjacent to the *CMPK1* promoter, as evidenced by high levels of H3K27Ac and p300/CBP (Fig. 3B) and enhancer reporter assays (fig. S8, A and B). Deletion of a ~400–base pair (bp) segment encompassing the boundary CTCF site, which abolished CTCF binding (fig. S8A), caused a factor of 2.3 induction of the *TAL1* transcript (Fig. 3C), which suggests that the integrity of the neighborhood contributes to the silent state of *TAL1* (Fig. 3D). In support of this model, contacts between DNA regions that are normally within and outside of the neighborhood were increased (Fig. 3, E and F, and fig. S10). Furthermore, deletion of the CTCF site in primary human T cells also caused a small but detectable activation of *TAL1* (fig. S8, C to G). These results are consistent with the idea that the silent state of the *TAL1* proto-oncogene is dependent on the integrity of the insulated neighborhood (Fig. 3D).

We further tested the model that site-specific perturbation of a loop boundary is sufficient to activate a proto-oncogene at the *LMO2* locus. The *LMO2* gene encodes a transcription factor that is overexpressed and oncogenic in some forms of T-ALL (*14*, *20*). The region upstream of the *LMO2* promoter is recurrently deleted in T-ALL, and these deletions are linked to *LMO2* activation (Fig. 3G); a previous study proposed that deletion of cryptic repressors located in the deleted region enables activation of *LMO2* (*21*). Analysis of a T-ALL patient cohort (*22*) revealed deletions that overlap the CTCF boundary site of the *LMO2* neighborhood, and patient cells harboring these deletions had generally high levels of *LMO2* expression (fig. S9, A and B). CRISPR/Cas9-mediated deletion in HEK-293T cells of a ~25-kb segment encompassing the insulated neighborhood boundary CTCF site and two additional CTCF sites that could act as boundary elements caused a factor of 2 increase in the *LMO2* transcript (Fig. 3, H to J) and a large-scale rearrangement of interactions around *LMO2*, as evidenced by chromosome conformation capture carbon copy (5C) analysis (Fig. 3, K and L, and fig. S10). These results indicate that the deleted CTCF sites contribute to the silent state of the *LMO2* proto-oncogene (Fig. 3J).

The boundaries of chromosome neighborhoods may be disrupted in other cancers. A recent study noted that mutations in CTCF binding sites occur frequently in cancers (*23*), but it is unclear whether mutations in boundaries are

common, as only a subset of CTCF sites form insulated neighborhoods (*8*, *10*, *24*). CTCF cohesin–bound loops are largely preserved across cell types (*8*, *9*, *24*), and a set of ~10,000 constitutive CTCF-CTCF loops shared by GM12878 lymphoblastoid, Jurkat, and K562 (CML) cells (*24*) were identified for comparison (Fig. 4A, fig. S11, and table S8). We used the International Cancer Genome Consortium (ICGC) database—which contains data for ~50 cancer types, ~2300 whole-genome sequence (WGS) samples, and ~13 million unique somatic mutations—to examine the boundaries of these neighborhoods for somatic point mutations found in cancer genomes (table S9). We found a striking enrichment of mutations at the CTCF boundaries of constitutive neighborhoods (Fig. 4B, fig. S12A, and table S10) relative to regions flanking the boundary CTCF sites (±1 kb of the CTCF binding motif; $P < 10^{-4}$, permutation test) (fig. S12B), and in many instances these created a change in the consensus CTCF binding motif (fig. S12C). Nonboundary CTCF sites did not show such enrichment (Fig. 4B and figs. S12D and S14). The genomes of esophageal and liver carcinoma samples were particularly enriched for boundary CTCF site mutations (Fig. 4, C and D, fig. S12, D and E, fig. S13, and table S10), and there was no similar enrichment of mutations at the binding sites of other transcription factors (fig. S15). In these cancers, a considerable fraction of the mutated neighborhood boundary CTCF sites were affected by multiple mutations (≥3 mutations per site) [280/1826 (15%) in esophageal carcinoma, 54/1030 (5%) in liver carcinoma] (table S10), and recurrent mutations occurred more frequently in neighborhood boundary CTCF sites relative to nonboundary CTCF sites (fig. S16, A to C). The genes located within the most frequently mutated neighborhoods included known cellular proto-oncogenes annotated in the Cancer Gene Census and other genes that have not been associated with these cancers (Fig. 4, E and F, and tables S11 and S12). Shown in Fig. 4, G and H, are two examples of proto-oncogene–containing neighborhoods where the activation of the gene located in the neighborhood has been observed in the respective cancer type. These results suggest that somatic mutations of insulated neighborhood boundaries occur in the genomes of many different cancers.

Our findings indicate that disruption of insulated neighborhood boundaries can cause oncogene activation in cancer cells. With maps of 3D chromosome structure such as those described here, cancer genome analysis can consider how recurrent perturbations of boundary elements may affect the expression of genes with roles in tumor biology. Our understanding of 3D chromosome structure and its control is rapidly advancing and should be considered for potential diagnostic and therapeutic purposes. Because control of 3D chromosome structure involves binding of specific sites by CTCF and cohesin, which is affected by protein cofactors, DNA methylation, and local RNA synthesis (*25*), advances in our understanding of these regulatory processes may provide new approaches to therapeutics that have an impact on aberrant chromosome structures.

REFERENCES AND NOTES

1. B. Vogelstein, K. W. Kinzler, *Nat. Med.* **10**, 789–799 (2004).
2. B. Vogelstein *et al.*, *Science* **339**, 1546–1558 (2013).
3. L. A. Garraway, E. S. Lander, *Cell* **153**, 17–37 (2013).
4. C. M. Croce, *N. Engl. J. Med.* **358**, 502–511 (2008).
5. M. H. Kagey *et al.*, *Nature* **467**, 430–435 (2010).
6. J. H. Gibcus, J. Dekker, *Mol. Cell* **49**, 773–782 (2013).
7. D. U. Gorkin, D. Leung, B. Ren, *Cell Stem Cell* **14**, 762–775 (2014).
8. J. M. Dowen *et al.*, *Cell* **159**, 374–387 (2014).
9. J. E. Phillips-Cremins *et al.*, *Cell* **153**, 1281–1295 (2013).
10. X. Ji *et al.*, *Cell Stem Cell* **18**, 262–275 (2016).
11. J. R. Dixon *et al.*, *Nature* **485**, 376–380 (2012).
12. E. P. Nora *et al.*, *Nature* **485**, 381–385 (2012).
13. S. A. Armstrong, A. T. Look, *J. Clin. Oncol.* **23**, 6306–6315 (2005).
14. P. Van Vlierberghe, A. Ferrando, *J. Clin. Invest.* **122**, 3398–3406 (2012).
15. M. J. Fullwood *et al.*, *Nature* **462**, 58–64 (2009).
16. Z. Tang *et al.*, *Cell* **163**, 1611–1627 (2015).
17. D. Hnisz *et al.*, *Cell* **155**, 934–947 (2013).
18. J. Lovén *et al.*, *Cell* **153**, 320–334 (2013).
19. L. Brown *et al.*, *EMBO J.* **9**, 3343–3351 (1990).
20. J. O'Neil, A. T. Look, *Oncogene* **26**, 6838–6849 (2007).
21. P. Van Vlierberghe *et al.*, *Blood* **108**, 3520–3529 (2006).
22. J. Zhang *et al.*, *Nature* **481**, 157–163 (2012).
23. R. Katainen *et al.*, *Nat. Genet.* **47**, 818–821 (2015).
24. N. Heidari *et al.*, *Genome Res.* **24**, 1905–1917 (2014).
25. C. T. Ong, V. G. Corces, *Nat. Rev. Genet.* **15**, 234–246 (2014).
26. C. G. Mullighan *et al.*, *Nature* **446**, 758–764 (2007).

ACKNOWLEDGMENTS

Supported by NIH grants HG002668 (R.A.Y.), CA109901 (R.A.Y.), NS088538 (R.J.), MH104610 (R.J.), and AI120766 (M.H.P.); an Erwin Schrödinger Fellowship (J3490) from the Austrian Science Fund (FWF) (D.H.); Ludwig Graduate Fellowship funds (A.S.W.); the Laurie Kraus Lacob Faculty Scholar Award in Pediatric Translational Research (M.H.P.); Hyundai Hope on Wheels (M.H.P.); and Danish Council for Independent Research, Medical Sciences, individual postdoctoral grant DFF–1333-00106B and Sapere Aude Research Talent grant DFF–1331-00735B (R.O.B.). Work in the Dekker lab is supported by the National Human Genome Research Institute (R01 HG003143, U54 HG007010, U01 HG007910), the National Cancer Institute (U54 CA193419), the NIH Common Fund (U54 DK107980, U01 DA 040588), the National Institute of General Medical Sciences (R01 GM 112720), and the National Institute of Allergy and Infectious Diseases (U01 R01 AI 117839). J.D. is an investigator of the Howard Hughes Medical Institute. We thank R. Fitzgerald, S. Grimmond, and the ICGC Genome Projects ESAD-UK and OV-AU for permission to use genome sequence data. Data sets generated in this study have been deposited in the Gene Expression Omnibus under accession number GSE68978. The Whitehead Institute filed a patent application based on this paper. R.A.Y. is a founder of Syros Pharmaceuticals, and R.J. is a founder of Fate Therapeutics.

SUPPLEMENTARY MATERIALS

www.sciencemag.org/content/351/6280/1454/suppl/DC1
Materials and Methods
Figs. S1 to S16
Tables S1 to S13
References (*27*–*71*)

19 November 2015; accepted 18 February 2016
Published online 3 March 2016
10.1126/science.aad9024

HIV-1 VACCINES

HIV-1 broadly neutralizing antibody precursor B cells revealed by germline-targeting immunogen

Joseph G. Jardine,[1,2,3]* Daniel W. Kulp,[1,2,3]* Colin Havenar-Daughton,[3,4]* Anita Sarkar,[2,3,5]* Bryan Briney,[1,2,3]* Devin Sok,[1,2,3]* Fabian Sesterhenn,[1]† June Ereño-Orbea,[6] Oleksandr Kalyuzhniy,[1,2,3] Isaiah Deresa,[3,4] Xiaozhen Hu,[1,3] Skye Spencer,[1,3] Meaghan Jones,[1,3] Erik Georgeson,[1,3] Yumiko Adachi,[1,2,3] Michael Kubitz,[1,2,3] Allan C. deCamp,[7] Jean-Philippe Julien,[2,3,5,6,8] Ian A. Wilson,[2,3,5,9] Dennis R. Burton,[1,2,3,10] Shane Crotty,[3,4,11]‡ William R. Schief[1,2,3,10]‡

Induction of broadly neutralizing antibodies (bnAbs) is a major HIV vaccine goal. Germline-targeting immunogens aim to initiate bnAb induction by activating bnAb germline precursor B cells. Critical unmet challenges are to determine whether bnAb precursor naïve B cells bind germline-targeting immunogens and occur at sufficient frequency in humans for reliable vaccine responses. Using deep mutational scanning and multitarget optimization, we developed a germline-targeting immunogen (eOD-GT8) for diverse VRC01-class bnAbs. We then used the immunogen to isolate VRC01-class precursor naïve B cells from HIV-uninfected donors. Frequencies of true VRC01-class precursors, their structures, and their eOD-GT8 affinities support this immunogen as a candidate human vaccine prime. These methods could be applied to germline targeting for other classes of HIV bnAbs and for Abs to other pathogens.

Development of an HIV vaccine is a global health priority. Recent discoveries of potent broadly neutralizing antibodies (bnAbs) that bind to relatively conserved epitopes on the HIV Env glycoprotein trimer and protect against challenge in animal models have reinvigorated vaccine design efforts to induce bnAbs (*1*). However, bnAbs have not been elicited in standard animal models or humans.

Germline targeting, a vaccine priming strategy to initiate the affinity maturation of select germline-precursor B cells, has promise to initiate

Activation of proto-oncogenes by disruption of chromosome neighborhoods
Denes Hnisz, Abraham S. Weintraub, Daniel S. Day, Anne-Laure Valton, Rasmus O. Bak, Charles H. Li, Johanna Goldmann, Bryan R. Lajoie, Zi Peng Fan, Alla A. Sigova, Jessica Reddy, Diego Borges-Rivera, Tong Ihn Lee, Rudolf Jaenisch, Matthew H. Porteus, Job Dekker and Richard A. Young (March 3, 2016)
Science **351** (6280), 1454-1458. [doi: 10.1126/science.aad9024]
originally published online March 3, 2016

Editor's Summary

The spread of bad neighborhoods

Our genomes have complex three-dimensional (3D) arrangements that partition and regulate gene expression. Cancer cells frequently have their genomes grossly rearranged, disturbing this intricate 3D organization. Hnisz *et al.* show that the disruption of these 3D neighborhoods can bring oncogenes under the control of regulatory elements normally kept separate from them (see the Perspective by Wala and Beroukim). These novel juxtapositions can result in the inappropriate activation of oncogenes.

Science, this issue p. 1454; see also p. 1398

Science (print ISSN 0036-8075; online ISSN 1095-9203) is published weekly, except the last week in December, by the American Association for the Advancement of Science, 1200 New York Avenue NW, Washington, DC 20005.